

RAIL JOINT MODEL BASED ON THE EULER-BERNOULLI BEAM THEORY

Traian Mazilu, Prof. PhD. Eng. University Politehnica of Bucharest, e-mail: trmazilu@yahoo.com

Ionuț Radu Răcănel, Assoc. Prof. PhD. Eng. Technical University of Civil Engineering Bucharest, e-mail: ionut_racanel@yahoo.com

Cristian Lucian Ghindea, Lect. PhD. Eng. Technical University of Civil Engineering Bucharest, e-mail: cristian.ghindea@utcb.ro

Radu Iuliu Cruciat, Lect. PhD. Eng. Technical University of Civil Engineering Bucharest, e-mail: rcruciat@utcb.ro

Mihai-Cornel Leu, PhD. Student Doctoral School of Transports, University Politehnica of Bucharest, e-mail: mihaileu.c@gmail.com

Rezumat

În acest articol este prezentat un model pentru joanta de cale ferată alcătuit din trei grinzi Euler-Bernoulli legate printr-o fundație Winkler cu scopul de a pune în evidență influența lungimii rostului de dilatație asupra rigidității joantei. Plecând de la rezultatele experimentale privind determinarea rigidității unui joante s-a calculat rigiditatea fundației Winkler a modelului. Utilizând modelul propus, s-a arătat că rigiditatea unei joante de șină 49 se reduce cu până la 10 % atunci când rostul de dilatație crește de la 0 la 20 mm.

Cuvinte cheie: joantă, eclisă, rost de dilatare, grindă Euler-Bernoulli, rigiditatea șină-eclisă, experiment, rigiditatea joantei

Abstract

In this paper, a rail joint model consisting of three Euler-Bernoulli beams connected via a Winkler foundation is proposed in order to point out the influence of the joint gap length upon the stiffness of the rail joint. Starting from the experimental results aiming the stiffness of the rail joint, the Winkler foundation stiffness of the model has been calculated. Using the proposed model, it is shown that the stiffness of the rail joint of the 49 rail can decrease up to 10 % when the joint gap length increases from 0 to 20 mm.

Keywords: rail joint, joint bar, joint gap, Euler-Bernoulli beam, distributed stiffness, testing, rail joint stiffness

1. INTRODUCTION

The jointed track was the first constructive solution to assure rails continuity and, despite of the disadvantage related to the weak points caused by the joints, this solution is still applied in the low-speed and load secondary lines due to the lower construction cost and the simpler equipment required for its installation and maintenance.

Figure 1 shows a rail joint for 49 rail type. Rail ends are connected to each other via two metal fish-plates or rail-joint bars (one on each part) and four bolts. A small gap between the rail ends is provided for dilatation reason. Also, the joint gap reduces the local stresses and helps to avoiding the buckling track.

The joint gap length depends on the rail length, rail temperature and fastener type. For example, according to the Romanian regulation [1], the joint gap length takes values between 0 and 20 mm.

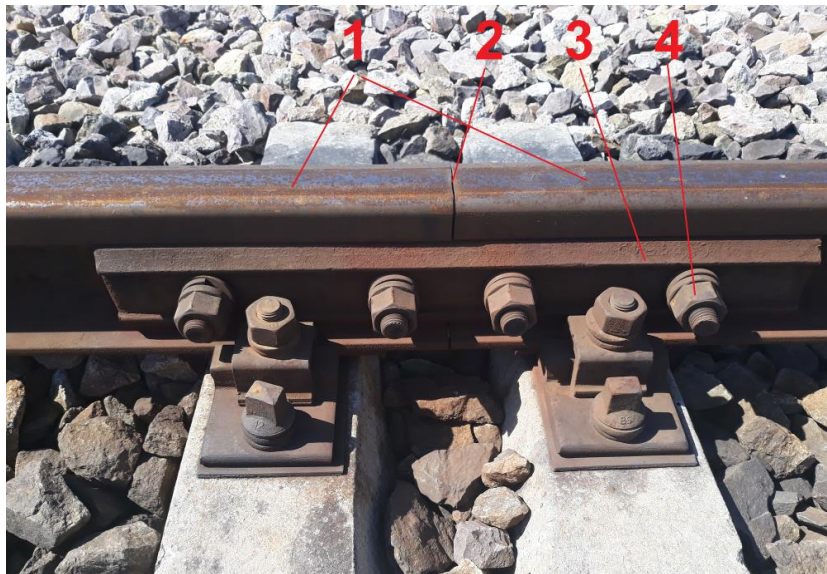


Figure 1. The 49 rail joint: 1. rail end; 2. joint gap; 3 joint bar; 4. bolt.

When trains are running along a jointed track, periodic shocks and a specific "clickety-clack" sound can be experienced. To identify the means of control of these undesirable effects, the wheel/rail joint interaction has been studied in the past and still represents an interesting research area. For instance, the wheel-rail joint contact geometry was investigated in [2], the elasto-plastic field in rail joint [3], wear of the rail joints [4], noise generated by jointed track [5], modelling and experiment [6].

In this paper, a rail joint model consisting in three Euler-Bernoulli beams connected via a Winkler foundation is presented. The model is like that proposed in [7], but this time, the solution to the equilibrium equations is simpler. The testing procedure to determine the distributed stiffness of the Winkler foundation is shown and the influence of the joint gap length is pointed out.

2. MECHANICAL MODEL OF THE RAIL JOINT

The mechanical model of a rail joint ensemble with joint gap including simply supported three Euler-Bernoulli beams system is presented in Figure 2. Two identical beams model the rail ends, and each of them has the length of $l + l_1$ (l – the length of the common part between the rail end and joint bar and l_1 – the distance from the joint bar to the support) and the bending stiffness EI_r , where E is Young's modulus and I_r – area moment of inertia of the cross section of the rail. The joint bars are modelled using an equivalent beam of length $2(l_0 + l)$, where $2l_0$ is the joint gap length, and the bending stiffness EI_b , where I_b is the area moment of inertia of the cross section of the two joint bars. The rail joint system has the length of $2L = 2(l_0 + l + l_1)$. Displacements of the rail ends are w_r for $0 \leq x \leq l$ and w_{r1} for $0 \leq x_1 \leq l_1$, and the displacements of the joint bars are w_{bo} for $0 \leq x_o \leq l_o$ and w_b for $0 \leq x \leq l$.

The connection between the rail ends and joint bars due to the bolts is modelled using a Winkler layer of length l for each rail end – joint bar assembly, and the linear stiffness k .

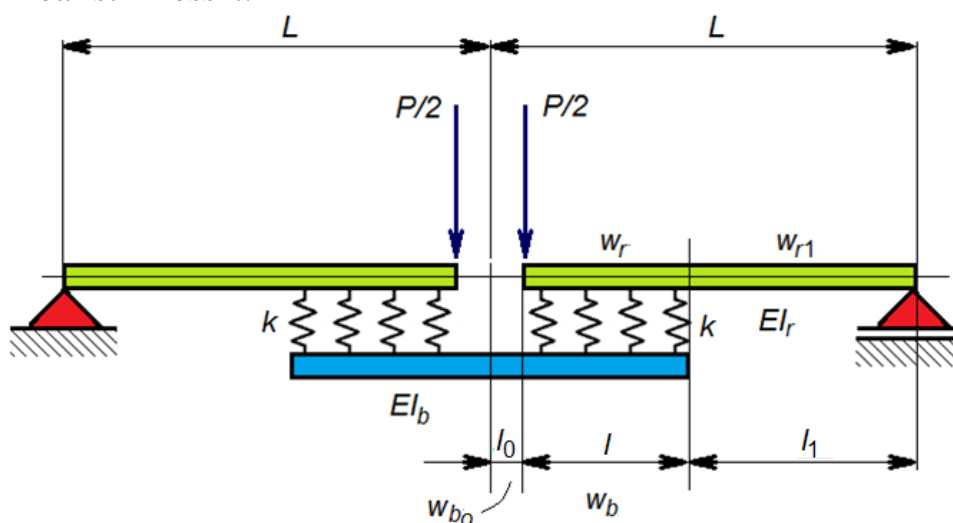


Figure 2. Mechanical model of the rail joint.

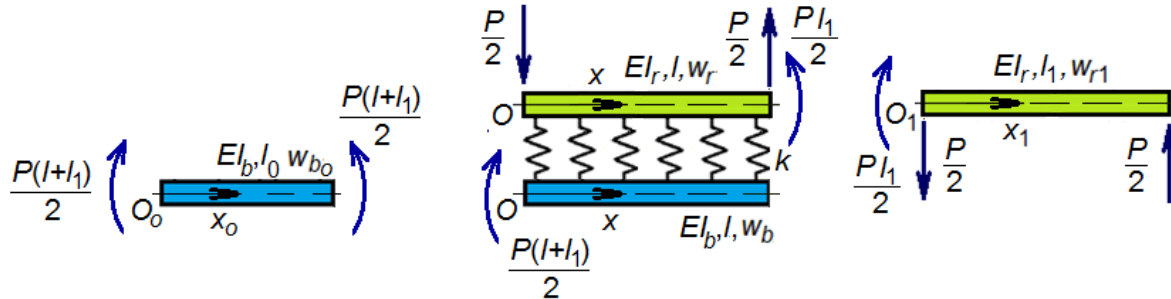


Figure. 3. Illustrative for the calculation of the rail joint displacement (right half of the model).

The rail joint ensemble is loaded with the vertical force $P/2$ on each rail end.

In the following lines, the deflection of the rail joint model is calculated using one half model from the symmetry reason.

Figure 3 shows the components of the right half of the rail joint model.

According to the Euler-Bernoulli beam theory and the loadings of the rail end and joint bar, the following equations hold:

- for joint bar

$$\frac{d^2 w_{bo}(x_o)}{dx_o^2} = -\frac{P}{2EI_b}(l+l_1), \quad 0 \leq x_o \leq l_0; \quad (1)$$

$$EI_b \frac{d^4 w_b(x)}{dx^4} + k[w_b(x) - w_r(x)] = 0, \quad 0 \leq x \leq l; \quad (2)$$

- for rail end

$$EI_r \frac{d^4 w_r(x)}{dx^4} + k[w_r(x) - w_b(x)] = 0, \quad 0 \leq x \leq l; \quad (3)$$

$$\frac{d^2 w_{r1}(x_1)}{dx_1^2} = -\frac{P}{2EI_r}(l_1 - x_1), \quad 0 \leq x_1 \leq l_1. \quad (4)$$

The next boundary conditions must be considered:

- for joint bar

$x_o = 0$, the slope of the beam is zero

$$\frac{dw_{bo}(0)}{dx_o} = 0 \quad (5)$$

$x_o = l_0$ and $x = 0$, the continuity conditions regarding the displacement and the slope, and the conditions related by the $P(l + l_1)/2$ bending moment and shear force which is zero

$$w_{bo}(l_0) = w_b(0), \quad \frac{dw_{bo}(l_0)}{dx_o} = \frac{dw_b(0)}{dx} \quad (6)$$

$$\frac{d^2w_b(0)}{dx^2} = -\frac{P}{2EI_b}(l + l_1), \quad \frac{d^3w_b(0)}{dx^3} = 0 \quad (7)$$

$x = l$, the bending moment and shear force are zero

$$\frac{d^2w_b(l)}{dx^2} = 0, \quad \frac{d^3w_b(l)}{dx^3} = 0 \quad (8)$$

- for rail end

$x = 0$, the bending moment is zero and the shear force is $-P/2$

$$\frac{d^2w_r(0)}{dx^2} = 0, \quad \frac{d^3w_r(0)}{dx^3} = \frac{P}{2EI_r} \quad (9)$$

$x = l$ and $x_1 = 0$, the continuity conditions regarding the displacement and the slope of the rail end

$$w_r(l) = w_{r1}(0), \quad \frac{dw_r(l)}{dx} = \frac{dw_{r1}(0)}{dx_1} \quad (10)$$

$x_1 = l_1$, the displacement is zero

$$w_{r1}(l_1) = 0. \quad (11)$$

The equations (2) and (3) can be rewritten as

$$\frac{d^8 w_{b,r}(x)}{dx^8} + 4\beta^4 \frac{d^4 w_{b,r}(x)}{dx^4} = 0, \quad (12)$$

where $4\beta^4 = \frac{k}{E} \frac{I_r I_b}{I_r + I_b}$.

The general solutions are

$$w_r(x) = A_1 ec(-\beta x) + A_2 es(-\beta x) + A_3 ec(\beta x) + A_4 es(\beta x) + A_5 x^3 + A_6 x^2 + A_7 x + A_8 \quad (13)$$

$$w_b(x) = B_1 ec(-\beta x) + B_2 es(-\beta x) + B_3 ec(\beta x) + B_4 es(\beta x) + B_5 x^3 + B_6 x^2 + B_7 x + B_8. \quad (14)$$

where $ec(\beta x) = e^{\beta x} \cos(\beta x)$ $es(\beta x) = e^{\beta x} \sin(\beta x)$. (15)

Inserting the two displacements in Eq. (2) or (3), it results that:

$$w_b(x) = -\frac{I_r}{I_b} [A_1 ec(-\beta x) + A_2 es(-\beta x) + A_3 ec(\beta x) + A_4 es(\beta x)] + A_5 x^3 + A_6 x^2 + A_7 x + A_8 \quad (16)$$

The solution to the equation (1) and the boundary condition (5) is

$$w_{bo}(x_0) = -\frac{P(l+l_1)}{4EI_b} x_0^2 + A_9, \quad (17)$$

And the solution to the equation (4) and the boundary condition (11) is

$$w_{r1}(x_1) = \frac{P}{12EI_r} x_1^3 - \frac{Pl_1}{4EI_r} x_1^2 + A_{10}(x_1 - l_1) + \frac{Pl_1^3}{6EI_r}. \quad (18)$$

Finally, from the boundary conditions (6 – 9) the following equations emerge

$$A_1 ec(0) + A_2 es(0) + A_3 ec(0) + A_4 es(0) - \frac{I_b}{I_r} A_8 + \frac{I_b}{I_r} A_9 = \frac{Pl_0^2(l+l_1)}{4EI_r} \quad (19)$$

$$A_1 ec'(0) + A_2 es'(0) + A_3 ec'(0) + A_4 es'(0) - \frac{I_b}{I_r} A_7 = \frac{Pl_0(l+l_1)}{2EI_r} \quad (20)$$

$$A_1 ec''(0) + A_2 es''(0) + A_3 ec''(0) + A_4 es''(0) - 2\frac{I_b}{I_r} A_6 = \frac{P(l+l_1)}{2EI_r} \quad (21)$$

$$A_1 ec'''(0) + A_2 es'''(0) + A_3 ec'''(0) + A_4 es'''(0) - 6\frac{I_b}{I_r} A_5 = 0 \quad (22)$$

$$A_1 ec''(-\beta l) + A_2 es''(-\beta l) + A_3 ec''(\beta l) + A_4 es''(\beta l) - 6\frac{I_b}{I_r} l A_5 - 2\frac{I_b}{I_r} A_6 = 0 \quad (23)$$

$$A_1 ec'''(-\beta l) + A_2 es'''(-\beta l) + A_3 ec'''(\beta l) + A_4 es'''(\beta l) - 6\frac{I_b}{I_r} A_5 = 0 \quad (24)$$

$$A_1 ec''(0) + A_2 es''(0) + A_3 ec''(0) + A_4 es''(0) + 2A_6 = 0 \quad (25)$$

$$A_1 ec'''(0) + A_2 es'''(0) + A_3 ec'''(0) + A_4 es'''(0) + 6A_5 = \frac{P}{2EI_r} \quad (26)$$

$$A_1 ec(\beta l) + A_2 es(\beta l) + A_3 ec(\beta l) + A_4 es(\beta l) + l^3 A_5 + l^2 A_6 + l A_7 + A_8 + l_1 A_{10} = \frac{Pl_1^3}{6EI_r} \quad (27)$$

$$A_1 ec'(\beta l) + A_2 es'(\beta l) + A_3 ec'(\beta l) + A_4 es'(\beta l) + 3l^2 A_5 + 2l A_6 + A_7 - A_{10} = 0. \quad (28)$$

The set of algebraic equations can be solved using a numeric method.

The parameters of the rail joint model can be determined by measurement (the length of the rail end and joint bar), and experiment – the stiffness of the rail end – joint bar connection. The inertia moments of the rail end and joint bar can be extracted from the rail documentation.

3. RAIL JOINT TESTING

In this section, the determination of the stiffness of the connection between the rail ends and joint bars, according to the previous model, is presented. To this end, the rail displacement in two sections on both sides of the gap is measured during the rail joint loading with the help of a universal hydraulic machine of maximum load of 400 kN, and then, the stiffness of the joint bars-rail ends connection is calculated using the rail joint model.



Figure 4. General view of the set-up of the rail joint testing.



Figure 5. Main components of the set-up of the rail joint testing: 1. rail end; 2. joint bar; 3. bolt; 4. joint gap; 5. support; 6. piercer; 7. displacement transducer.

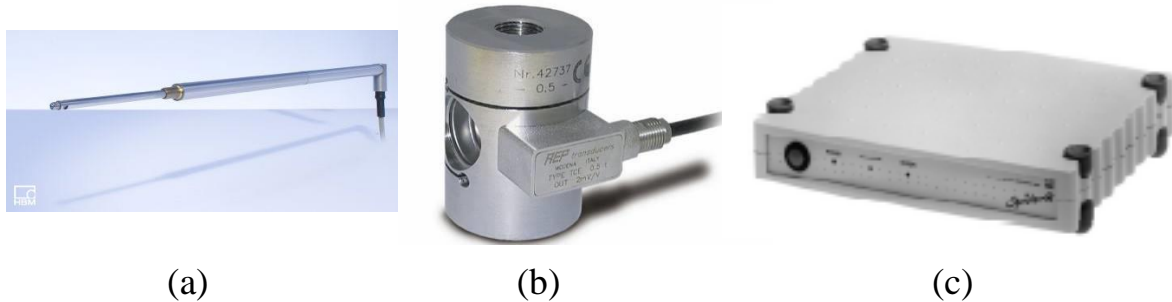


Figure 6. Components of the measuring chain:
(a) displacement transducer WA 20; (b) force inductive transducer TCE-TM of 100 kN; (c) data bridge 'SPIDER 8'.

Figures 4 and 5 show the testing set-up for a rail joint probe of 1200 mm length for the 49 rail; the length of the gap is 7 mm.

To measure the displacement of the rail ends, two WA 20 inductive displacement transducers with the 20 mm measuring base were used (Figure 6 a). The loading force was measured using a TCE-TM 100 kN inductive force transducer (Figure 6 b). 8-channel "SPIDER 8" data acquisition station (Hottinger Baldwin Messtechnik) was used for data processing to ensure amplification of the signal and transmission to the storage unit (Figure 6 c).

The measurement system was assisted by a portable computer that works with the "CATMAN AP" software (Hottinger Baldwin Messtechnik), used for the processing, representation and storage of experimentally measured data.

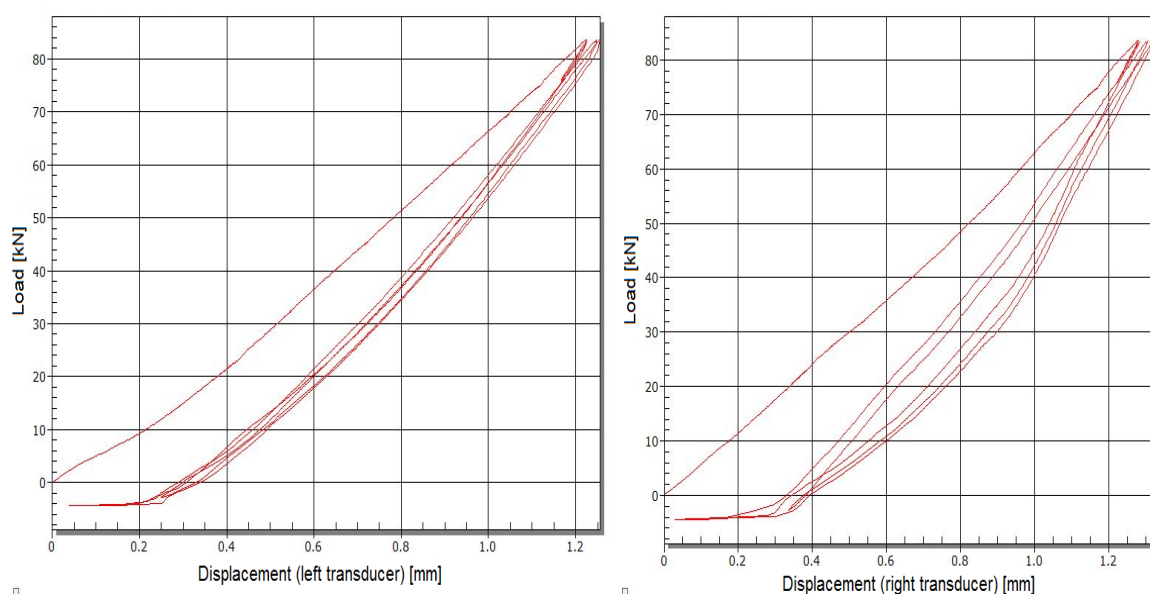


Figure 7. Force-displacement diagrams.

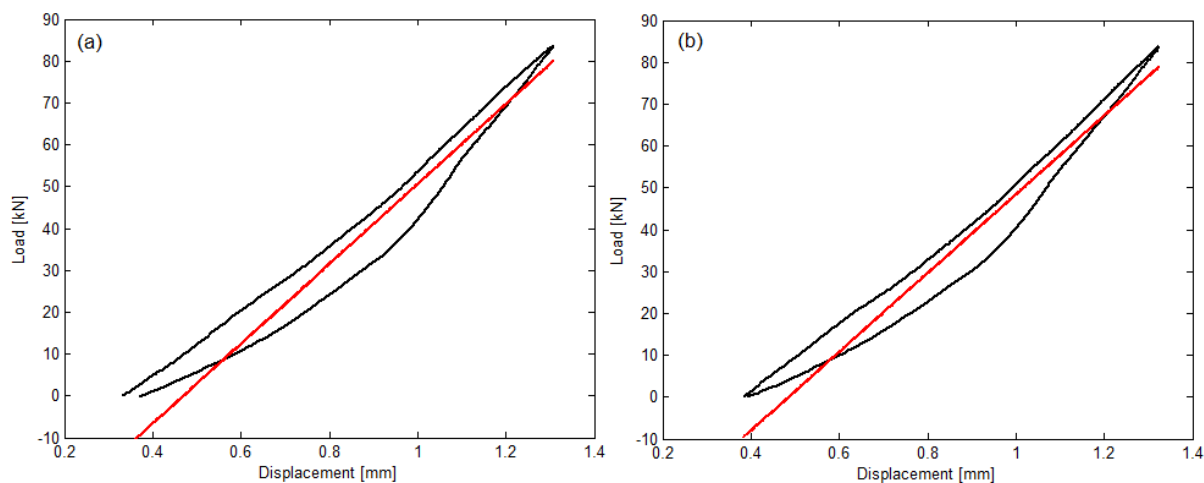


Figure 8. Force-displacement diagrams for the left transducer: black line – from measurement; red line – from theory; (a), first cycle; (b), second cycle.

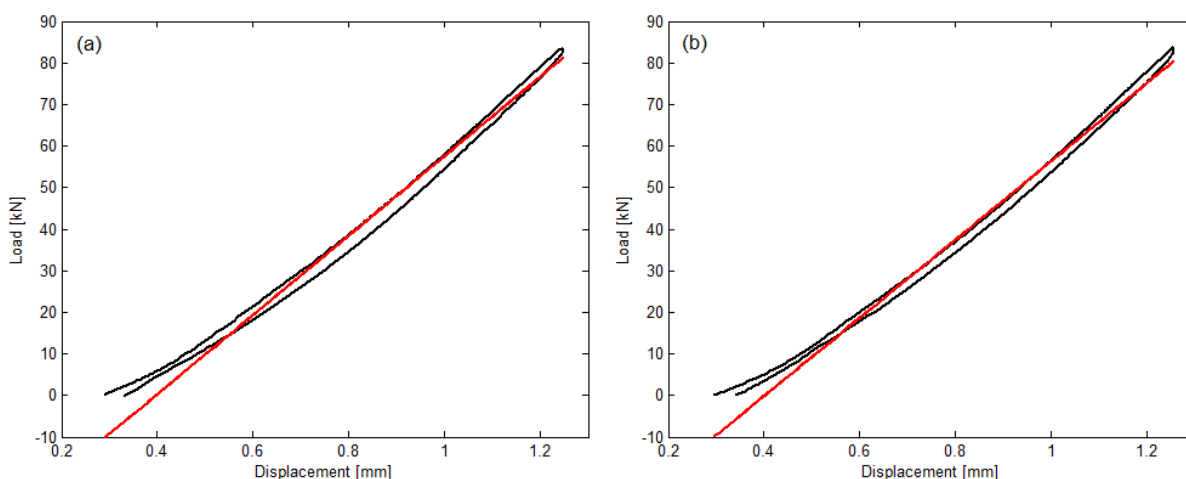


Figure 9. Force-displacement diagrams for the right transducer: black line – from measurement; red line – from theory; (a), first cycle; (b), second cycle.

Three loading-unloading cycles were performed at a maximum force of approximately 83 kN and the diagrams obtained are shown in Figure 7. It is interesting to show that after the first loading / unloading cycle, all curves are stabilized.

Figures 8 and 9 exhibit the two loading-unloading cycles stabilized for the left and right transducers. Theoretical results are also presented as a linear variation. These were obtained by applying the least squares method.

The slope of the load-displacement theoretical lines represents the ratio between the load and rail displacement in the transducer section (Fig. 10). In the following lines, it is named the rail joint stiffness, according to the equation

$$k_{rj} = \frac{P}{w_r(a)}. \quad (29)$$

The rail joint stiffness takes closed value: 95,52 and 94,13 kN/mm for the left transducer and 95,41 and 93,99 kN/mm for the right transducer. Mean value of the load-displacement slopes is 94,73 kN/mm and this value is retained to determine the distributed stiffness between joint bars and rail ends.

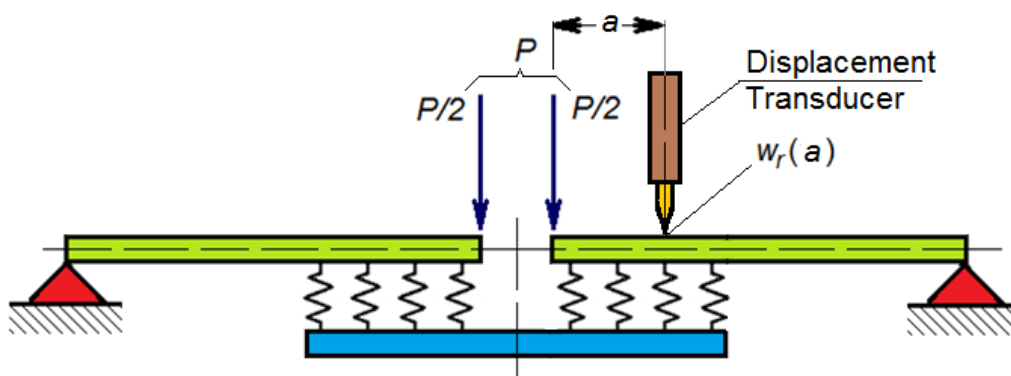


Figure. 10. Explicative for the slope of the load-displacement diagram.

Figure 11 shows the rail joint stiffness (Eq. 29) depending on the distributed stiffness between rail bars and rail ends. The following parameters have been considered: distance between supports $2L = 1$ m, position of the displacement transducer, $a = 60$ mm and the parameters of the rail joint of 49 rail: $E = 2,1 \cdot 10^{11}$ Pa, $I_r = 18,19 \cdot 10^{-6}$ m⁴, $I_b = 2 \cdot 1,635 \cdot 10^{-6}$ m⁴ and $L_b = 630$ mm. Finally, results the distributed stiffness between joint bars and rail ends of 872.26 GPa.

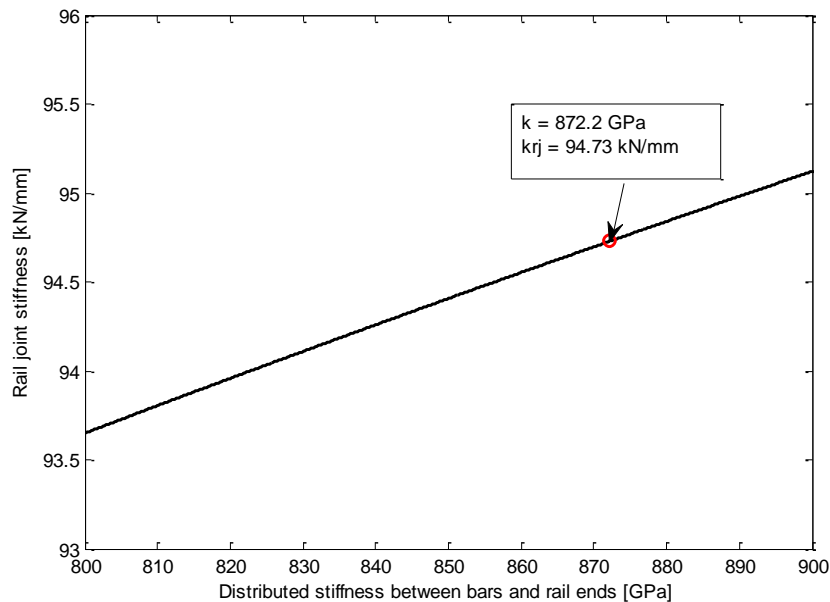


Figure 11. Determination of the distributed stiffness between bars and rail ends.

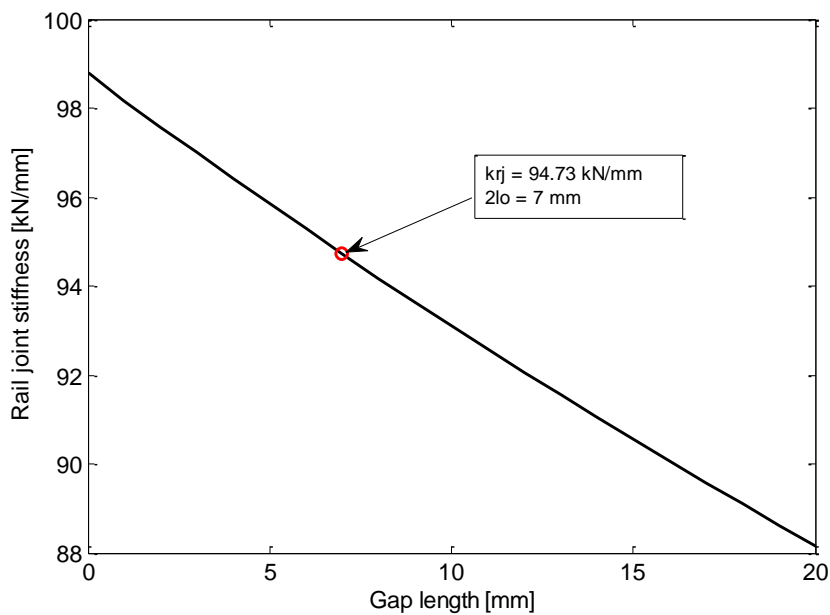


Figure 12. Rail joint stiffness versus gap length.

Figure 12 exhibits the influence of the gap length upon the rail joint stiffness (Eq. 29). The maximum gap length is 20 mm, according to the regulation at CFR [1]. The rail joint stiffness decreases from 98.8 kN/mm when the rail joint has no gap to 88.2 kN/mm for the gap length of 20 mm.

5. CONCLUSIONS

The particularity of the joint track is the rail joints itself, which is the connection between the ends of the rail coupons with the help of the joint bars attached with metal bolts. Rail joint is the weakest part of the joint track and is the main source of undesirable vibrations and shocks.

In this paper an analytical model of the rail joint, consisting of three Euler-Bernoulli beams interconnected by a Winkler layer, allowing to simulate the influence of the joints gap upon the rail joint stiffness, is presented. The experimental procedure based on the rail joint model for determining the distributed stiffness of the linkage between joint bars and rail ends is presented. This is applied to the 49-rail joint and the value of 836 GPa is obtained.

Starting from the model of the rail joint and the distributed stiffness between joint bars and rail ends, it is shown that the rail joint stiffness can decrease up to 10 % when the gap length increases from 0 to 20 mm, respectively from the minimum to maximum allowed value. This new aspect has not been revealed yet and it is interesting from the view point of the vehicle/joint track interaction prediction. Therefore, future research is focused on embodying this model into the vehicle/joint track model.

REFERENCES

- [1]. 314 Instruction, *Rules and tolerances for track construction and maintenance*, **1989**.
- [2]. T. MAZILU, M. DUMITRIU, C. TUDORACHE, M. SEBEȘAN: “*Wheel-rail joint geometry*”, Proceedings of 4th International Workshop on Soft Computing Applications, pp. 259-263, **2010**.
- [3]. W. CAI, Z. WEN, X. JIN, W. ZHAI: “*Dynamic stress analysis of rail joint with height difference defect using finite element method*”, Engineering Failure Analysis, Vol. 14, pp. 1488-1499, **2007**.
- [4]. Y. C. CHEN, L.W. CHEN: “*Effects of insulated rail joint on the wheel/rail contact stresses under the condition of partial slip*”, Wear, Vol. 260, pp. 1267-1273, **2006**.
- [5]. T. X. WU, D.J. THOMPSON: “*On the impact noise generation due to a wheel passing over rail joints*”, Journal of Sound and Vibration, Vol. 267, pp. 485-496, **2003**.
- [6]. M. OREGUI: “*Vertical Railway Track Dynamics: from Measurements to Numerical Modelling*”, Doctoral thesis, TU Delft, **2015**.

- [7]. T. MAZILU, M. C. LEU, “*On the Modelling of Rail Joint*”, Materials Science Forum, Vol. 957, pp. 33-42, **2019**.